JCAMECH

Vol. 48, No. 1, June 2017, pp 53-64
DOI: 10.22059/jcamech.2017.232927.142

Multi objective optimization of the vibration analysis of composite natural gas pipelines in nonlinear thermal and humidity environment under non-uniform magnetic field

A. Moradi[1,2*], H. Makvandi[3], I. Bavarsad Salehpoor[4, 5]

[1] *School of Mechanical Engineering, College of Engineering, University of Shahid Chamran Ahvaz, Iran*

[2] *School of Mechanical engineering ,Ahvaz Branch, Islamic Azad University ,Ahvaz ,Iran*

[3] *School of Mechanical engineering ,Abadan Branch, Islamic Azad University ,Abadan ,Iran*

[4] *School of Industrial Engineering, Amirkabir University of Technology, Tehran, Iran*

[5] *School of Industrial Engineering ,Masjed-Soleiman Branch, Islamic Azad University ,Masjed-Soleiman ,Iran*

Received: 8 May. 2017, Accepted: 15 June. 2017

Abstract
Adhesive In the field of fluid structure interactions fluid conveying pipe is a basic dynamical problem. In recent years considerable attention has been given to the lateral vibrations of pipes containing by a moving fluid. In this article, the vibration analysis of composite natural gas pipeline in the thermal and humidity environment is studied. The effect of the non-uniform magnetic field is investigated. The equation of motion is derived by applying the Hamilton's principle for the pipe with the effects of both linear and nonlinear stress temperature cases. The differential quadrature method (DQM) has been utilized in computing the results for the fluid conveying pipe. The Bees algorithm and Genetic algorithm NSGA II for multi-objective optimization of a pipe model are used. Sample results are presented for several cases with varying values of the system parameter. Results are demonstrated for the dependence of natural frequencies on the flow velocity as well as temperature change and humidity percent. The effect of temperature change on critical flow velocity which causes to occur buckling instability is investigated. It is summarized that the influence of temperature change on the instability of fluid conveying pipe is significant.

Keywords: Composite pipes; Fluid-induced vibration; Thermal load; Humidity environment, Multi objective optimization, Magnetic field

[*] Corresponding Author. Tel.: +989163302402
Email Address: a.moradi64@gmail.com

1. Introduction

Since the problem of fluid conveying pipes is very important in industrial applications, the vibration and stability of fluid conveying pipes have been studied for a long time. Examples of such problems are flow-induced vibration of a pipeline supported above ground level, as well as conveying internal flow. Describing the vibration characteristics of the Trans-Arabian pipeline was first made by Ashley and Haviland, which is worth to mention in this area. Paidoussis et al. studied the linear and nonlinear dynamics of cantilevered cylindrical pipes with axial flow. They pointed out that the primary cause of loses of stability by divergence was the increase of flow velocity. Recently, the nonlinear dynamics of axially moving beams have attracted much attention [1]. However, to the best of authors' knowledge, the literature dealing with the behavior of fluid-conveying pipes under thermal loads is very limited. Therefore, studying the stability and dynamics of fluid-conveying pipes under thermal loads is felt necessary. Newly, the mechanical behavior of the mechanical structures, like the beam and plate, which are located in the magnetic field, was investigated by some of the researchers [2, 3]. To this end, some of the experimental studies were done on the nanobeam under an electro-magnetic field [4-8]. The effect of the longitudinal magnetic fields was considered in the wave propagation analysis of the nanobeam by Kiani [8]. In this paper, the nonlocal continuum theory was applied to obtain the governing equation to analyze the vibration of single layer graphene sheet. The effect of an in-plane magnetic field on the transverse vibration of a single-layer graphene sheet was considered by Murmu et al. [9]. In this paper, the nonlocal continuum theory was applied to obtain the governing equation to analyze the vibration of single layer graphene sheet.

The aim of an optimization problem is to find a combination of independent parameters to minimize or maximize a single or several quantities subjected to some limitations. The quantity to be optimizes is referred to as objective function. If only one function has to be optimized, the problem is a single function optimization problem and if more functions than one are involved it is a multi-objective optimization problem. Since most engineering design problems require having multi objective functions to be optimized, there is an increasing interest in multi-objective optimization algorithms. There are two approaches to dealing with multi-objective optimization problems.

The first approach is to form a linear combination of objective functions with different weights and to solve the resulting function by a method which is applied to a single function optimization problem. The second approach –the genuine one- is to consider all the objective-functions simultaneously. There are two main drawbacks in combining all objective functions into one. One problem is that all the solutions may not be found and the second problem is that some of the weights assigned to objective functions may be inappropriate, thus some of the functions involved in the problem would lose their effect in the final result. In engineering design problems, it is of interest to find, not only a single optimal solution, but all the possible solutions in a multi-objective problem which are called a Pareto-optimal set. None of the solutions in a Pareto-optimal solution set is better than the others, they are not comparable and each one is called a feasible solution. Different techniques to solve multi objective optimization problems are discussed in reference [10]. The authors have developed a new technique which is called Bees Algorithm [11] and they have applied it to constrained and unconstrained single objective problems. A modified version of Bees Algorithm has been created to identify as many non-dominated solutions as possible. In most of engineering design problems constraints are very important, since they impose limitations on the search space that makes the search process troublesome and inefficient.

The interest of the present study is the vibration analysis of fluid-conveying pipes under thermal loads in the different boundary conditions. Also, the effect of the humidity changes on the vibration frequencies and critical velocity is investigated. Furthermore, in this work, the Bees algorithm [11, 12] and Genetic algorithm NSGA II are applied to optimize the multi-objective fitness functions of a pipe model. The conflicting objective functions which are weight (W) and natural frequency (ω) have been considered for minimization and maximization. The pipe length (L), outer diameter (Dout), inner diameter (Din), fluid velocity (u) are design parameters applied in the optimization of vibration. In this work, the equation of motion is derived by the Hamilton's principle in which the thermal effect and humidity effect is considered. The thermal loads with both linear and non-linear thermo-elastic relations are developed. Two objective functions are used in this paper: the first objective function concerned to minimize the entire weight of pipe, and second objective function concern to maximize natural frequency. This study would be helpful to design the transmission fluid pipelines especially natural gas and oil pipelines.

2. Mathematical Modeling

2.1. *The principle of Hamilton*

The derivation is initiated by considering a representative element (P_f), with the length of dx, as shown in Fig. 1.The fluid moves along the y-axis (see Fig. 1 for the coordinate system) with velocity of $V = \frac{\partial y}{\partial t} + U_g \frac{\partial y}{\partial x}$ inside the pipe, and the pipe itself moves in the direction y with velocity $\frac{\partial y}{\partial t}$. The kinetic energy of the system is

$$T = \frac{1}{2}\left(\int_0^L \left(\iint_{A_g} \rho_g \left(\frac{\partial y}{\partial t} + U_g \frac{\partial y}{\partial x}\right)^2 dA_g\, dx\right) + \int_0^L I \left(\frac{\partial y}{\partial t}\right)^2 dx\right) \quad (1)$$

where the densities of the natural gas are namely ρ_g , ρ_p, pipe's material, respectively; $A_g = \frac{\pi D_{in}^2}{4}$ and $I = \sum_{k=1}^{N} \pi \rho^{(k)} (r_{k+1}^2 - r_k^2)$ are the cross-section areas of gas and pipe mass per unit length, respectively; D_{in} and D_{out} are the inside and outside diameters of the pipe respectively (see Fig. 1); U_g is the velocity of the moving gas (in the x-direction).

The work done by the pre-tension (T) and the distributed forces (q), can be written as

$$\delta W_1 = \int_0^L T \frac{\partial^2 y}{\partial x^2} \delta y\, dx + \int_0^L q\, \delta y\, dx \quad (2)$$

where the pre-tensioning force in the pipe is T and the work done by the gas through shear friction and pressure can be written as

$$\delta W_2 = \int_0^L 2\, \rho_g A_g U_g^2\, f \frac{L}{D_g} \frac{\partial^2 y}{\partial x^2} \delta y\, dx + \int_0^L P(1 - 2\vartheta\delta) A_g\, \delta y \frac{\partial^2 y}{\partial x^2} \delta y\, dx \quad (3)$$

Where P is the gas pressure. The internal pressurization makes an additional tensile force which is equal to $-2\vartheta P A_g$ for a thin pipe if the downstream end is not free to flow axially, or even not completely free, where t is the Poisson's ratio of the pipe. Thus, the equivalent pressure can be expressed in a general formula form as $P(1 - 2\vartheta\delta)A_g$, in which $\delta = 0$ indicates that there is no constraint to the axial flow of at the downstream end, otherwise $\delta = 1$.

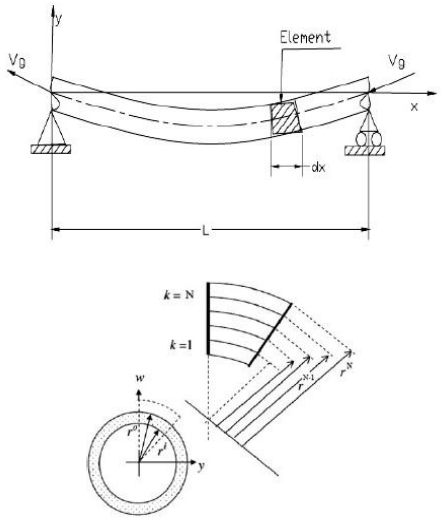

Figure 1: A fluid-conveying pipe with pinned ends at sub-sea and the coordinate system [13].

In Eq. (3) f is the Fenning friction factor, which can be approximated by

$$\frac{1}{\sqrt{f}} = -4 \log\left(\frac{\frac{k}{D_g}}{3.7065} + \frac{1.2613}{Re\sqrt{f}}\right), \quad Re = \frac{\rho_g D_g U_g}{\mu} \quad (4)$$

where Re is the Reynolds number, μ is the gas viscosity, k is the absolute pipe roughness and D_g is the internal diameter of the pipe. The strain energy of the dx segment of the pipe can be represented by

$$\prod = \frac{1}{2}\int_0^L \left(\aleph \left(\frac{\partial^2 y}{\partial x^2}\right)^2 + N\left(\frac{\partial y}{\partial x}\right)^2\right) dx + \int_0^L \frac{A}{2E^k}\left(E^k \frac{\partial \vartheta}{\partial x} - \gamma(\Delta T)\right)^2 dx, \quad \aleph = \sum_{k=1}^{N} E^k (r_{k+1}^4 - r_k^4) \quad (5)$$

Where v is the longitudinal displacements, and $\gamma(\Delta T)$is the stress–temperature coefficient, which is a function of ΔT. The N is divided to two parts Nth and NH that these terms are caused by the temperature change and the moisture change,

respectively. These terms are obtained as following form

$$N^{th}(x) = -\int_A \varphi(\Delta T)dA, \qquad N^H(x) = -\sum \frac{\pi}{4} E^k \beta^k (r_{k+1}^2 - r_k^2)\Delta H \tag{6}$$

In this study, the linear and nonlinear elastic stress temperature coefficients are considered. The linear stress temperature is defined as [14]

$$\varphi(\Delta T) = \sum_{k=1}^{N} E^k \alpha^k \Delta T, \qquad N^{th} = \sum_{k=1}^{N} \frac{\pi}{4} E^k \alpha^k (r_{k+1}^2 - r_k^2)\Delta T \tag{7}$$

The nonlinear elastic stress temperature coefficient is defined as [14]

$$\varphi(\Delta T) = \sum_{k=1}^{N} E^k \alpha^k \Delta T - h^* \left(\alpha^{(k)}\right)^2 \Delta T^2, \qquad N^{th} = \sum_{k=1}^{N} \begin{pmatrix} E^k \alpha^k \Delta T \\ -h^* (\alpha^{(k)})^2 \Delta T^2 \end{pmatrix} (r_{k+1}^2 - r_k^2)$$

$$h^* = \sum_{k=1}^{N} \begin{Bmatrix} h_1\left(1 - 2\vartheta^k\right) - 2h_2\left(\left(\vartheta^k\right)^2 - 1\right) \\ +h_3\left(\left(\vartheta^k\right)^2\right. \end{Bmatrix} \tag{8}$$

In the above equation, the terms h_1, h_2 and h_3 are Murghana's constants [14]. The Hamilton's principle statement in the absence of dissipative forces can be formulated for supported fluid-conveying pipes as follows

$$\delta L = \delta \int_{t_1}^{t_2} (T + W - \Pi)dt \tag{9}$$

Substituting the expressions (1)–(3) into the above equation, the equations of motion is

$$\aleph \frac{\partial^4 y}{\partial x^4} + \begin{pmatrix} P(1 - 2\nu\delta)A_g - T \\ -2I_g f U_g^2 \frac{L}{D_g} + N^{th} + N^h \end{pmatrix} \frac{\partial^2 y}{\partial x^2} + 2I_g U_g^2 \frac{\partial^2 y}{\partial x\, \partial t} + q + \left(I_g + I\right)\frac{\partial^2 y}{\partial t^2} = 0, \quad I_g = \rho_g A_g \tag{10}$$

For the pipe, the boundary conditions of SS, CS, and CC are given, respectively, by

$$y(0) = \frac{\partial^2 y}{\partial x^2}(0) = 0;\ y(l) = \frac{\partial^2 y}{\partial x^2}(l) = 0$$
$$y(0) = \frac{\partial y}{\partial x}(0) = 0;\ y(l) = \frac{\partial y}{\partial x}(l) = 0$$
$$y(0) = \frac{\partial y}{\partial x}(0) = 0;\ y(l) = \frac{\partial^2 y}{\partial x^2}(l) = 0 \tag{11}$$

2.2. *Maxwell's relations*

In this part, we intend to calculate the effect of magnetic field on the dynamic behavior of fluid conveyed pipe. To this end, we express the characteristic electro-dynamic Maxwell equations for a completely conducting elastic body as follows form [2, 8]

$$\nabla \times e = -\eta \frac{\partial h}{\partial t};\quad \nabla . h = 0;\quad e = -\eta\left(\frac{\partial U}{\partial t} \times \overline{H}\right); h = \nabla \times (U \times H)\, J = \nabla \times h \tag{12}$$

In the above equations, the components U, η and J are introduced as the vector of displacement, magnetic field permeability and the current density, respectively. Moreover, e is a strength vector of electric field and h is a disturbing magnetic field vector [2, 8]. In this study, we assume that the Nano beam is located in one direction non-uniform magnetic field. Also, the displacement vector is stated as U=(u,v,w), then

$$h = \nabla \times (U \times H) = -H_x\left(\frac{\partial v}{\partial y} + \frac{\partial w}{\partial z}\right)\hat{\imath} + \left(H_x \frac{\partial v}{\partial x} + \frac{\partial H_x}{\partial x} v\right)\hat{\jmath} + \left(H_x \frac{\partial w}{\partial x} + \frac{\partial H_x}{\partial x} w\right)\hat{k}$$

$$J = \nabla \times h = \begin{pmatrix} H_x\left(-\frac{\partial^2 v}{\partial x\, \partial z} + \frac{\partial^2 w}{\partial x\, \partial y}\right) + \frac{\partial H_x}{\partial x}\left(\frac{\partial w}{\partial y} - \frac{\partial v}{\partial z}\right) \\ +\frac{\partial H_x}{\partial y}\frac{\partial w}{\partial x} - \frac{\partial H_x}{\partial z}\frac{\partial v}{\partial x} + \frac{\partial^2 H_x}{\partial x\, \partial y} w - \frac{\partial^2 H_x}{\partial x\, \partial z} v \end{pmatrix}, -\left(H_x\left(\frac{\partial^2 v}{\partial y\, \partial z} + \frac{\partial^2 w}{\partial x^2} + \frac{\partial^2 w}{\partial z^2}\right) + 2\frac{\partial H_x}{\partial x}\frac{\partial w}{\partial x} + \frac{\partial H_x}{\partial z}\frac{\partial v}{\partial y} + \frac{\partial H_x}{\partial z}\frac{\partial w}{\partial z} + \frac{\partial^2 H_x}{\partial x^2} w\right)\hat{\jmath} \tag{13}$$

$$+(H_x\left(\frac{\partial^2 v}{\partial x^2}+\frac{\partial^2 v}{\partial y^2}+\frac{\partial^2 w}{\partial y\,\partial z}\right)+2\frac{\partial H_x}{\partial x}\frac{\partial v}{\partial x}+\frac{\partial H_x}{\partial y}\frac{\partial v}{\partial y}+\frac{\partial H_x}{\partial y}\frac{\partial w}{\partial z}+\frac{\partial^2 H_x}{\partial x^2}\,v)\hat{k}$$

Due to the magnetic field, an exerted body force is applied on the pipe. This force is named the Lorentz force; also, this force is shown by the notation f. The Lorentz force is calculated as follows form

$$f = f_x\hat{\imath} + f_y\hat{\jmath} + f_z\hat{k} = \eta(J \times H) \tag{14}$$

In this study, we consider that the pipe is located in the longitudinal varying magnetic field; thus, in the above equation, we insert $H_x = H_0 \sin(\pi x/l)$that it shows the magnetic field varies as sinusoidal respect to the x direction. As mentioned, the magnetic field causes to produce the Lorentz force. Consequently, the Lorentz force is caused to act the transverse load on the pipe. This force is obtained by using the Eq. (14), therefore the transverse force can be represented as [2, 8]

$$q_{magnetic} = \int_A f_z\,dA$$
$$= \eta\,A\,H_0^2 \sin^2\left(\frac{\pi x}{l}\right)\frac{\partial^2 w}{\partial x^2} + 2\eta A\,\frac{\pi}{l}\,H_0^2 \sin^2\left(\frac{\pi x}{l}\right)\cos\left(\frac{\pi x}{l}\right) - \eta\,A\,H_0^2\left(\frac{\pi}{l}\right)^2 \sin^2\left(\frac{\pi x}{l}\right) w \tag{15}$$

In this work, it is assumed that the pipe is located in a longitudinal magnetic field. Therefore, in the Eq. (10) the transverse load $q(x,t)$ is induced by the magnetic field and is stated$q(x,t) = q_{magnetic}$. So by substituting the Eq. (15) into the Eq. (10) the motion differential equation is obtained for transverse displacement (w=y) as follows form;

$$\aleph\,\frac{\partial^4 y}{\partial x^4} + \begin{pmatrix} P(1-2\nu\delta)A_g - T \\ -2I_g f\,U_g^2\,\frac{L}{D_g} + N^{th} + N^h \end{pmatrix}\frac{\partial^2 y}{\partial x^2} + 2I_g U_g^2\,\frac{\partial^2 y}{\partial x\,\partial t} + \eta\,A\,H_0^2 \sin^2\left(\frac{\pi x}{l}\right)\frac{\partial^2 y}{\partial x^2} + 2\eta A\,\frac{\pi}{l}\,H_0^2 \sin^2\left(\frac{\pi x}{l}\right)\cos\left(\frac{\pi x}{l}\right)\frac{\partial y}{\partial x} - \eta\,A\,H_0^2\left(\frac{\pi}{l}\right)^2 \sin^2\left(\frac{\pi x}{l}\right) y + (I_g + I)\frac{\partial^2 y}{\partial t^2} = 0$$
$$I_g = \rho_g A_g \tag{16}$$

3. Solution by differential quadrature method

To solve the Eq. (10), if it is not impossible to solve the governing equation as the exact form, it is very difficult to find a solution as exact form. To this end, we search to find a numerical solution to solve the Eq. (10). For this purpose, the differential quadrature method (DQM) is selected and there are two important reasons for choice this method. The first, the DQM is a powerful numerical technique to solve the governing equation of the mechanical structures [15-17]. This method has low computational cost in comparison with the other numerical method such as the finite element method, the finite difference method and etc. The second, the DQM obtain results with high accuracy in comparison with other numerical technique [15]. The readers can find the other advantages of the DQM in the Refs [15, 18-20]. Therefore, in this paper, the DQM is applied to discrete the Eq. (10) and boundary conditions in the Eq. (11). The fundamental idea of differential quadrature method is that the derivative of a function with regards to a space variable at a given sampling point is approximated as a weighted linear sum of the sampling points in the domain of that variable. There are described how to use DQM to solve motion partial differential equations and are explained in detail how to apply boundary conditions in the Ref [19, 21]; so, we refer the readers to see the details to the Refs [16, 19, 21-31]. In this approach, at a given grid point x, the derivatives of a function can be approximated as

$$\left.\frac{\partial^m W}{\partial \xi^m}\right|_{x=x_i} = \sum_{k=1}^{N_x} C_{ik}^{(m)}\,W(\xi_k,t) = \sum_{k=1}^{N_x} C_{ik}^{(m)}\,W_{kj}(t) \tag{17}$$

Where the nmber of grid points along the ξ-direction is N_x. The notation is introduced as the m-th order weight coefficients. uTo determine the r-th order weight coefficients, one must obtain the first order weight coefficients. These coefficients are determined by the Lagrange interpolated polynomial as the following form [17]

$$C_{ij}^{(1)} = \begin{cases} \dfrac{M(\xi_i)}{(\xi_i - \xi_j)M(\xi_j)} & \text{for } i \neq j \\ -\displaystyle\sum_{j=1,i\neq j}^{N_\xi} C_{ij}^{(1)} & \text{for } i = j \end{cases} \tag{18}$$

In the equation (18), $C_{ij}^{(1)}$ and $M(\xi)$ are the Lagrange polynomial and the first order weight coefficient, respectively. The $M(\xi_i)$ is obtained by the Lagrange polynomial as the following form

$$M(\xi_i) = \prod_{j=1, i\neq j}^{N_\xi} (\xi_i - \xi_j) \tag{19}$$

As mentioned, in the DQM, the higher order weight coefficients are used to approximate higher order derivatives of the function and the higher order coefficients are calculated by the first order weight coefficients as the following form

$$C_{ij}^{(r)} = r\left[C_{ij}^{(r-1)}\, C_{ij}^{(1)} - \frac{C_{ij}^{(r-1)}}{(\xi_i - \xi_j)}\right] \quad \text{For } i, j = 1,2,\dots,N_\xi,\ i \neq j \ \text{ and } \ 2 \leq r \leq N_\xi - 1$$

$$C_{ij}^{(r)} = \sum_{j=1, i\neq j}^{N_\xi} C_{ij}^{(r)} \quad \text{for } i = 1,2,\dots,N_\xi \ \text{ and } \ 1 \leq r \leq N_\xi - 1 \tag{20}$$

Here, the notation$C_{ij}^{(r)}$) is the r-th order weight coefficients. The DQM results are very sensitive to mesh grid points and there are several sets of the mesh grid points. One of the grid point sets is the non-uniform grid points and it was shown that this grid point set gives the results with good accuracy and low computational cost in comparison with other grid point sets. For this purpose, in this paper, we choose these set of grid points in terms of natural coordinate directions ξ as

$$\xi_i = \frac{1}{2}\left(1 - \cos\left(\frac{(i-1)\pi}{(N_\xi - 1)}\right)\right) \tag{21}$$

After implementation of the boundary conditions, the Eq. (10) is rewritten in the DQM terms as the following form

$$[M]\{\ddot{d}\} + [C]\{\dot{d}\} + [K]\{d\} = 0 \tag{22}$$

In the equation (22), the matrices M, C and K are the mass, damper and stiffness matrix, respectively. By defining the new freedom vector and general solution of the Eq. (10) as the following form

$$\{Q\} = \begin{Bmatrix} d \\ \dot{d} \end{Bmatrix}, \qquad y(x,\tau) = \{Q\}\, e^{\eta\tau} \tag{23}$$

By using the Eq. (22), we can rewrite the Eq. (23) as

$$\eta A\{\dot{Q}\} + B\{Q\} = 0, \quad A = \begin{bmatrix} 0 & M \\ I & 0 \end{bmatrix}, \quad B = \begin{bmatrix} K & C \\ 0 & -I \end{bmatrix} \tag{24}$$

In the above equation, η is a complex number and pipe vibration frequency is the imaginary part of it. After the implementation of the Eq. (10) in the DQM form, the elements of stiffness, mass and damper matrix are given in the Eq. (25), respectively.

$$\begin{aligned} K &= \aleph \sum_{k=1}^{N_\xi} C_{ik}^{(4)}\, W_{k,j} + P(1-2\nu\delta)\sum_{k=1}^{N_\xi} C_{ik}^{(2)}\, W_{k,j} - T\sum_{k=1}^{N_\xi} C_{ik}^{(2)}\, W_{k,j} + \sum_{k=1}^{N_\xi} \sin^2(\pi\xi_i) C_{ik}^{(2)}\, W_{k,j} \\ &+ 2\eta A H_0^2 \sum_{k=1}^{N_\xi} \sin(\pi\xi_i)\cos(\pi\xi_i) C_{ik}\, W_{k,j} - \eta A H_0^2 \left(\frac{\pi}{l}\right)^2 \sum_{k=1}^{N_\xi} \sin^2(\pi\xi_i)\, W_{k,j} \\ &- 2 I_g f U_g^2 \frac{l}{D} \sum_{k=1}^{N_\xi} C_{ik}^{(2)}\, W_{k,j} + N^{th}\sum_{k=1}^{N_\xi} C_{ik}^{(2)}\, W_{k,j} + N^{h}\sum_{k=1}^{N_\xi} C_{ik}^{(2)}\, W_{k,j} \\ C &= 2 I_g U_g^2 \frac{l}{D} \sum_{k=1}^{N_\xi} C_{ik}^{(1)}\, W_{k,j}, \qquad M = (I_g + I) W_{k,j} \end{aligned} \tag{25}$$

4. Multi objective optimization problems

Solving multi-objective optimization problems, finally, give rise to a system of Pareto–optimal solutions, so, Evolutionary Algorithms (EAs) are ideal to handle this kind of problems. To have an effective search, it is necessary to guide the search toward the Pareto-optimal set. Prevention of premature saturation and a well distributed population in Pareto front are also two important issues in the search process. Pioneering work in context of Evolutionary Algorithms has been performed by Schaffer [32]; other significant developments are explained in the works by Fonseca and Fleming [33], Horn et al [34], Knowles et al [35], Zitzler et al

[36]and Deb et al [37]. Mathematically, multi-objective optimization problems can be stated as

$$\text{Minimize } y = \{f_1(x), f_2(x), f_3(x), \dots f_M(x)\}$$

$$\text{Subject to } g(x) = \{g_1(x), g_2(x), g_3(x), \dots g_J(x)\} \leq 0$$

$$h(x) = \{h_1(x), h_2(x), h_3(x), \dots h_k(x)\} = 0$$

$$\text{Where } x = \{x_1, x_2, x_3, \dots, x_N\} \in X$$

$$y = \{y_1, y_2, y_3, \dots, y_N\} \in Y \quad (26)$$

X is the vector of decision variables, y is the objective vector, X is the decision space, and Y is called objective space .The solution of Eq. (26) usually is not unique, but a set of equally efficient, no inferior, non-dominated solutions which are named as Pareto-optimal set. A no inferior solution is one that is not overcome by any other possible solution. For the maximization case, mathematically, it is said that solution x^1 dominates x^2 or x^1 is superior to x^2 when

$$\forall i \in \{1,2, \dots, M\} \quad , \quad y(x^1) \geq y(x^2) \quad \forall i \in \{1,2, \dots, M\} \mid y_i(x^1) > y_i(x^2) \quad (27)$$

If any x is not dominated by any other one, then it is a non-inferior, non-dominated or Pareto-optimal point. Two points in a Pareto-optimal set are indifferent to each other. If any of Pareto-optimal solutions is found then the optimization algorithm should be terminated, but it is of interest to achieve all Pareto-optimal solutions because, fitness of each one depends on number of factors such as: designer's choice, practical restrictions and project limitations. Bees Algorithm is explained in the following section in detail.

4.1. *The Steps of Bees Algorithm*

The Bees Algorithm (BA) is a search method which is inspired by the foraging behavior of honey bees. This section summarizes the main steps of the Bees Algorithm. For more details reader is referred to references [11, 12, 38]. Table.1 shows the pseudo code for the Bees Algorithm in its simplest form which is dependent to some parameters described in Table.2.

Table 1: Parameters of the Bees Algorithm

Population	$\boldsymbol{n}$
Number of selected sites	m
Number of top-rated sites out of m selected sites	e
Number of bees recruited for best e sites	n_{ep}
Number of bees recruited for the other (m-e) selected sites	n_{sp}
Initial patch size	n_{gh}
Number of iteration	i_{max}

Table 2: Pseudo code of the Bees Algorithm

1-Initialize population with random solutions.
2-Evaluate fitness of the population
3-While (stopping criterion not met) // forming new population.
4-Select sites for neighborhood search and determine the path size
5-Recruit bees for selected sites (more bees for best e sites) and evaluate fitness
6-Select the fitness bees from each path
7-Amend the Pareto optimal set
8- Assign remaining bees to search randomly and evaluate their fitness's
1-End While

4.2. *Define Optimization Problem*

The objective functions of the optimization process are J_1 and J_2. The first criteria, J_1 is the total weight of pipe and the second criteria, J_2 is the natural frequency. The constraint of problem (g1) checks the ratio of outer diameter to the length of pipe in order to keep assuming of optimization problem formulated as

$$\text{Minimize} \quad J_1 = 2\pi\rho Lg \frac{D_{out}+D_{in}}{2} \times \frac{D_{out}-D_{in}}{2} \quad \text{Minimize} \quad J_2 = -\omega \quad \text{Subjected to:} \quad g_1 = \frac{D_{out}}{L} < 0.1$$

$$\text{Where,} \quad 0.5 < L < 5 \qquad 0.15 < D_{out} < 0.35 \qquad 0.1 < D_{in} < 0.3 \qquad 0 < u < 3$$

5. Results and discussions

5.1. *Vibration Results*

In this part, in order to illustrate the prominent features of the mechanical behavior of fluid conveyed

pipe, the selected numerical results are presented, as well as the effects of humidity percentage and temperature effect. The material property constants have been reported by Ref. [13]. To indicate the minimum number of grid points for convergence analysis of the DQM, a MATLAB code is written based on the Eq. (19). It is based on the fact that the DQM results are sensitive to lower grid points. To obtain the results of the convergence analysis, the pipe is studied by considering the fluid velocity, the temperature change, the humidity percentage, the length of the pipe and the radius, 10 m/s, 30, 10% and 1 m, respectively. To show the convergence analysis, the error percent is defined as follow:

$$\text{Vibration error percent} = \left|\frac{\text{df}}{\text{cr}}\right| \times 100$$

Here, the df is vibration present results-vibration converged results and the cr is converged vibration frequency. The vibration frequency error percent against the number of grid points are shown in the Figure 2. In accordance with Figure 2, present solution is convergent. From the figure it is obviously shown that the tenth number of grid points ($N_\xi = 10$) are adequate to gain the accurate solutions for the present analysis.

There are no published papers in the present class of problem; thus, the numerical solutions which are obtained in this study compare with those results presented by Zou et al. [13]. To this end, the gas velocity, the thermal change, the effect of the magnetic field and the humidity change are ignored. According to the Table 3, the present results are in good agreement with those reported by Zou et al [13].

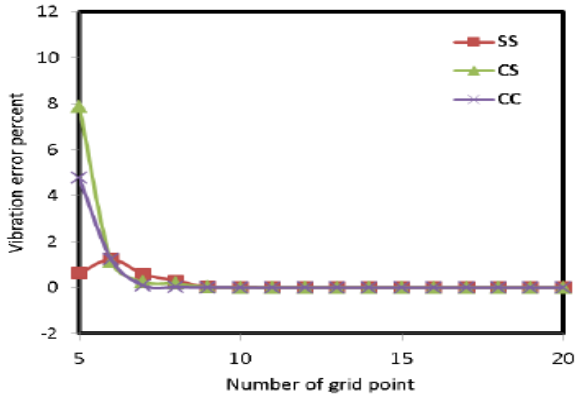

Figure 2: Convergence study and minimum number of grid points (N_ξ) required to obtain accurate the vibration frequency for four different boundary conditions.

Table 3: Comparison of natural frequency obtained from the present model with some known results available in the literature.

Mode	Structural frequency (Hz)			
	Pipe without pressure		Pipe with 3 Mpa pressure	
	Present	Ref. [13]	Present	Ref. [13]
1	0.2630	0.2630	0.0000	0.0000
2	1.6480	1.6480	1.1003	1.1003
3	4.6144	4.6144	4.0907	4.0907
4	9.0424	9.0424	8.4016	8.4016

In this section, the effect of gas speed on vibration frequency is investigated. The Figure 3 shows the effect non-dimensional gas velocity ($U_g l\sqrt{(\rho_f A_f)/\aleph}$) on the non-dimensional vibration frequency $\text{Im}(\mu) l^2\sqrt{(\rho_f A_f + \rho_p A_p)/\aleph}$ of the pipe for the various values of the temperature change. To plot this figure, the numerical results are based on the assumptions that the pipe length and the boundary condition are 1 m and SS, respectively. The Figure 3 shows the effects of the temperature change and the gas velocity on the natural frequency of the pipe. The gas velocity has a diminishing effect on the vibration frequency of pipe. In the other words, the vibration frequency of pipe is decreased by the increasing of the gas velocity. Moreover, this figure shows the critical velocity of the laminate pipe. The pipe is buckle when the vibration of the pipe is vanished. In this figure, the intersection points on the vibration curves with the gas velocity axis are shown the critical velocity. This interesting phenomenon can be expressed by this fact that the gas velocity causes that the pipe becomes more flexible and by increasing the temperature change, the pipe rigidity factor becomes smaller and when the gas velocity reach to the critical velocity the rigidity factor is set to zero and the laminate pipe is buckled. Also, it is clearly seen that if the temperature change becomes larger the critical velocity keep on to decreasing. The same results have been seen for other boundary conditions. Thus, it is deduced that the temperature change has a significant role in the vibration and buckling behavior of laminate fluid conveyed gas pipe and this factor must be considered to design the transmission gas pipelines.

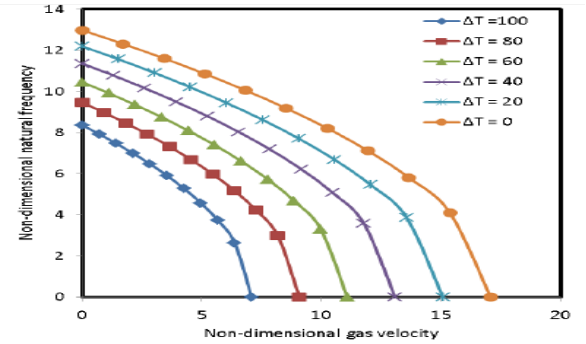

Figure 3: Change of the non-dimensional natural frequency of the pipe versus the non-dimensional gas velocity for various temperature changes.

To show the effect of the nonlinearity of the thermal stress and comparison it with the linear thermal stress, the vibration frequency against the temperature change for the nonlinear thermal stress and linear thermal stress is illustrated in the Fig. 4. To this end, the temperature change varies from 0 to 100 K. From this figure, it is clear that the vibration frequency reduces with enhancing the temperature change. It is based on the fact that the pipe becomes more flexible in the thermal environment; thus, the temperature change has a reduction effect on the stiffness matrix of the pipe. Also, it is evidently that the nonlinear thermal stress curve and the linear thermal stress curve are farther away from each other with increasing the temperature change. Consequently, the vibration frequencies of the nonlinear thermal stress case are smaller than the vibration frequencies obtained linear thermal stress case.

To show the importance of the humidity change on the vibration frequency of Nano-beam, the humidity difference percentage is defined as follow.

$$\mathrm{Hdp} = \left| \frac{\mathrm{Vf}_{\Delta \mathrm{H}=50\%} - \mathrm{Vf}_{\Delta \mathrm{H}=0}}{\mathrm{Vf}_{\Delta \mathrm{H}=0}} \right| \times 100$$

Here the Hdp and Vf are humidity difference percentage and vibration frequency, respectively. To this end, the humidity difference percentage versus the temperature change is illustrated in the Fig. 5. This figure is plotted for different boundary conditions. From this figure, it is evidently that the humidity difference percentage increases with increase the temperature change for all of the boundary conditions. Consequently, the humidity change has important effect on the vibration frequency of the fluid conveyed pipe with temperature change in comparison with the pipe without temperature change. Another point to consider is that, as the stiffness of the boundary condition increases the effect of the humidity percentage on the vibration frequency decreases.

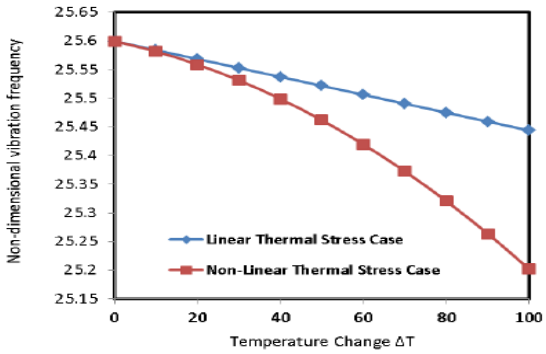

Figure 4: Change of non-dimensional vibration frequency with temperature change for linear and nonlinear thermal stress cases.

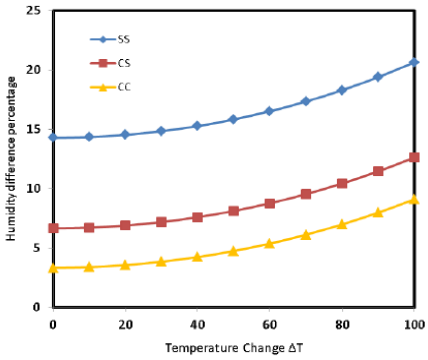

Figure 5: Change of humidity difference percentage with nonlocal parameter for various boundary conditions.

5.2. *Optimization results*

This section includes two parts. The first part gives the best parameters for the present models with Bees algorithm method and Genetic Algorithm NSGA II while the second part deals with simulation of present optimally designed pipe. Given the conflicting objective functions, the optimization algorithms clearly did not give rise to an optimum set-up, but to a Pareto frontier including several set-ups. The reverse tendency of some parameters was verified. On the other hand, as compared to the initial, previously manually optimized set-up, some important improvements are achieved. The optimization approach provided obvious indications for the optimum values of input variables, especially with regards to minimum weight and maximum natural frequency. The actual figures verified important improvements of the most of parameters. The empirically chosen parameters for the optimization are given in the Table 4. Figures 6 and 7 show the non-dominated solutions obtained using Bees Algorithm and Genetic Algorithm for pipe respectively. It is clear that Bees Algorithm can find

more non-dominated solutions than non-dominated genetic algorithm.

Table 4: Parameters of the Bees Algorithm for optimization of pipe

n	m	e	n_{ep}	n_{sp}	n_{gh}	i_{max}
50	20	4	20	15	0.01	200

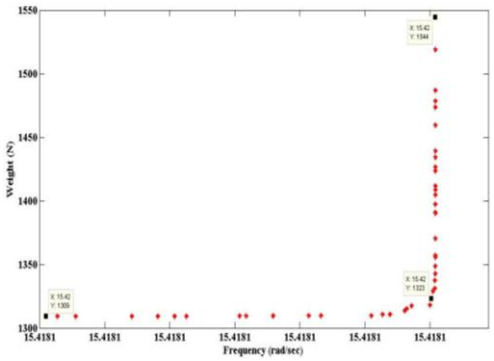

Figure 6: Non-dominated solutions obtained for optimization using BA Algorithm.

Table 5 shows that Bees Algorithm and NSGA II.

It is an advantage of Bees Algorithm, Compared to Other optimization methods.

Table 5: Optimization results for conveyed pipe by using BA algorithm.

Point	L	D_{in}	D_{out}	U	Weight	Frequency
	NSGAII algorithm results					
A	1.7702	0.0528	0.1538	0.0150	1309.8703	15.41812103
B	1.7723	0.0517	0.1540	0.0142	1323.0236	15.41813028
C	1.7752	0.0356	0.1606	0.0141	1544.4307	15.41813087
	BA algorithm results					
A	1.5402	0.0345	0.15	0.6679	1163.8658	15.25068529
B	1.8347	0.0542	0.1733	0.3263	1762.4634	15.37839394
C	2.9478	0.0855	0.2094	0	3819.0194	15.41820571

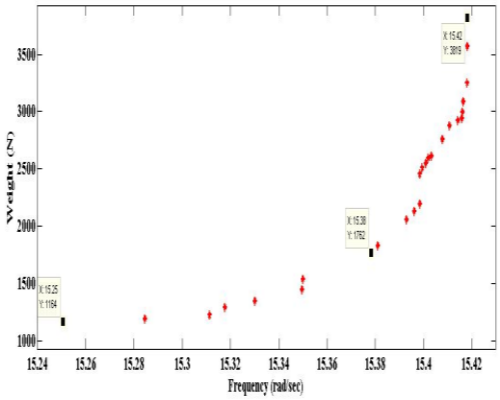

Figure 5: Non-dominated solutions obtained for optimization using GA Algorithm.

6. Conclusion

The vibration analysis of the fluid conveying pipe has been investigated by considering the effects of humidity and temperature changes. The effect of non-uniform magnetic field on the vibration behavior of fluid conveying pipe is also considered. Moreover, the linear and nonlinear thermal stress cases are studied in this work. Then, the Bees algorithm and NSGA II for multi-objective optimization of a pipe model to minimize total weight and maximize the natural frequency of pipe are applied. From the results of the present study, the following conclusions are noticeable:

1. The natural frequency of pipe depends on the flow velocity as well as temperature change and humidity percent.
2. The influence of temperature change on the instability of fluid conveying pipe is significant.
3. The simulation results unveil the robust performance of the proposed optimization approach based on the BA technique to minimize total weight and maximize the natural frequency of pipe.

7. References

[1] M. H. Ghayesh, M. Amabili, Post-buckling bifurcations and stability of high-speed axially moving beams, *International Journal of Mechanical Sciences*, Vol. 68, pp. 76-91, 2013.

[2] A. Arani, M. Maboudi, A. G. Arani, S. Amir, 2D-magnetic field and biaxiall in-plane pre-load effects on the vibration of double bonded orthotropic graphene sheets,

J Solid Mech, Vol. 5, No. 2, pp. 193-205, 2013.

[3] S. Narendar, S. Gupta, S. Gopalakrishnan, Wave propagation in single-walled carbon nanotube under longitudinal magnetic field using nonlocal Euler–Bernoulli beam theory, *Applied Mathematical Modelling*, Vol. 36, No. 9, pp. 4529-4538, 2012.

[4] K. Bubke, H. Gnewuch, M. Hempstead, J. Hammer, M. L. Green, Optical anisotropy of dispersed carbon nanotubes induced by an electric field, *Applied physics letters*, Vol. 71, No. 14, pp. 1906-1908, 1997.

[5] X. Liu, J. L. Spencer, A. B. Kaiser, W. M. Arnold, Electric-field oriented carbon nanotubes in different dielectric solvents, *Current Applied Physics*, Vol. 4, No. 2, pp. 125-128, 2004.

[6] E. Camponeschi, R. Vance, M. Al-Haik, H. Garmestani, R. Tannenbaum, Properties of carbon nanotube–polymer composites aligned in a magnetic field, *Carbon*, Vol. 45, No. 10, pp. 2037-2046, 2007.

[7] P. Lu, L. He, H. Lee, C. Lu, Thin plate theory including surface effects, *International Journal of Solids and Structures*, Vol. 43, No. 16, pp. 4631-4647, 2006.

[8] K. Kiani, Transverse wave propagation in elastically confined single-walled carbon nanotubes subjected to longitudinal magnetic fields using nonlocal elasticity models, *Physica E: Low-dimensional Systems and Nanostructures*, Vol. 45, pp. 86-96, 2012.

[9] T. Murmu, M. McCarthy, S. Adhikari, In-plane magnetic field affected transverse vibration of embedded single-layer graphene sheets using equivalent nonlocal elasticity approach, *Composite Structures*, Vol. 96, pp. 57-63, 2013.

[10] K. Deb, S. Agrawal, A. Pratap, T. Meyarivan, A fast elitist non-dominated sorting genetic algorithm for multi-objective optimization: NSGA-II, in *Proceeding of*, Springer, pp. 849-858.

[11] D. Pham, A. Ghanbarzadeh, E. Koc, S. Otri, S. Rahim, M. Zaidi, The bees algorithm-A novel tool for complex optimisation, in *Proceeding of*, sn, pp.

[12] D. Pham, A. Ghanbarzadeh, Multi-objective optimisation using the bees algorithm, in *Proceeding of*.

[13] G. Zou, N. Cheraghi, F. Taheri, Fluid-induced vibration of composite natural gas pipelines, *International journal of solids and structures*, Vol. 42, No. 3, pp. 1253-1268, 2005.

[14] T. Je¸ kot, Nonlinear problems of thermal postbuckling of a beam, *Journal of Thermal Stresses*, Vol. 19, No. 4, pp. 359-367, 1996.

[15] M. Mohammadi, M. Ghayour, A. Farajpour, Free transverse vibration analysis of circular and annular graphene sheets with various boundary conditions using the nonlocal continuum plate model, *Composites Part B: Engineering*, Vol. 45, No. 1, pp. 32-42, 2013.

[16] M. Mohammadi, M. Goodarzi, M. Ghayour, S. Alivand, Small scale effect on the vibration of orthotropic plates embedded in an elastic medium and under biaxial in-plane pre-load via nonlocal elasticity theory, 2012.

[17] M. Mohammadi, A. Farajpour, M. Goodarzi, Numerical study of the effect of shear in-plane load on the vibration analysis of graphene sheet embedded in an elastic medium, *Computational Materials Science*, Vol. 82, pp. 510-520, 2014.

[18] H. Asemi, S. Asemi, A. Farajpour, M. Mohammadi, Nanoscale mass detection based on vibrating piezoelectric ultrathin films under thermo-electro-mechanical loads, *Physica E: Low-dimensional Systems and Nanostructures*, Vol. 68, pp. 112-122, 2015.

[19] S. Asemi, A. Farajpour, H. Asemi, M. Mohammadi, Influence of initial stress on the vibration of double-piezoelectric-nanoplate systems with various boundary conditions using DQM, *Physica E: Low-dimensional Systems and Nanostructures*, Vol. 63, pp. 169-179, 2014.

[20] M. Mohammadi, A. Farajpour, M. Goodarzi, F. Dinari, Thermo-mechanical vibration analysis of annular and circular graphene sheet embedded in an elastic medium, *Latin American Journal of Solids and Structures*, Vol. 11, No. 4, pp. 659-682, 2014.

[21] M. Mohammadi, A. Farajpour, M. Goodarzi, R. Heydarshenas, Levy type solution for nonlocal thermo-mechanical vibration of orthotropic mono-layer graphene sheet embedded in an elastic medium, *Journal of Solid Mechanics*, Vol. 5, No. 2, pp. 116-132, 2013.

[22] M. Mohammadi, M. Ghayour, A. Farajpour, Analysis of free vibration sector plate based on elastic medium by using new version

differential quadrature method, *Journal of solid mechanics in engineering*, Vol. 3, No. 2, pp. 47-56, 2011.

[23] M. Safarabadi, M. Mohammadi, A. Farajpour, M. Goodarzi, Effect of surface energy on the vibration analysis of rotating nanobeam, *Journal of Solid Mechanics*, Vol. 7, No. 3, pp. 299-311, 2015.

[24] A. Farajpour, M. H. Yazdi, A. Rastgoo, M. Mohammadi, A higher-order nonlocal strain gradient plate model for buckling of orthotropic nanoplates in thermal environment, *Acta Mechanica*, Vol. 227, No. 7, pp. 1849-1867, 2016.

[25] M. Mohammadi, M. Safarabadi, A. Rastgoo, A. Farajpour, Hygro-mechanical vibration analysis of a rotating viscoelastic nanobeam embedded in a visco-Pasternak elastic medium and in a nonlinear thermal environment, *Acta Mechanica*, Vol. 227, No. 8, pp. 2207-2232, 2016.

[26] M. Goodarzi, M. Mohammadi, A. Farajpour, M. Khooran, Investigation of the effect of pre-stressed on vibration frequency of rectangular nanoplate based on a visco pasternak foundation, *Journal of Solid Mechanics*, Vol. 6, pp. 98-121, 2014.

[27] S. R. Asemi, M. Mohammadi, A. Farajpour, A study on the nonlinear stability of orthotropic single-layered graphene sheet based on nonlocal elasticity theory, *Latin American Journal of Solids and Structures*, Vol. 11, No. 9, pp. 1515-1540, 2014.

[28] M. Mohammadi, A. Farajpour, M. Goodarzi, H. Mohammadi, Temperature effect on vibration analysis of annular graphene sheet embedded on visco-pasternak foundation, *J. Solid Mech*, Vol. 5, pp. 305-323, 2013.

[29] M. Goodarzi, M. Mohammadi, M. Khooran, F. Saadi, Thermo-Mechanical Vibration Analysis of FG Circular and Annular Nanoplate Based on the Visco-Pasternak Foundation, *Journal of Solid Mechanics Vol*, Vol. 8, No. 4, pp. 788-805, 2016.

[30] M. R. Farajpour, A. Rastgoo, A. Farajpour, M. Mohammadi, Vibration of piezoelectric nanofilm-based electromechanical sensors via higher-order non-local strain gradient theory, *Micro & Nano Letters*, Vol. 11, No. 6, pp. 302-307, 2016.

[31] A. Farajpour, A. Rastgoo, M. Mohammadi, Vibration, buckling and smart control of microtubules using piezoelectric nanoshells under electric voltage in thermal environment, *Physica B: Condensed Matter*, 2017.

[32] J. D. Schaffer, Multiple objective optimization with vector evaluated genetic algorithms, in *Proceeding of*, LawrenceErlbaumAssociates, Inc., Publishers, pp.

[33] C. M. Fonseca, P. J. Fleming, Genetic Algorithms for Multiobjective Optimization: FormulationDiscussion and Generalization, in *Proceeding of*, Citeseer, pp. 416-423.

[34] J. Horn, N. Nafpliotis, D. E. Goldberg, A niched Pareto genetic algorithm for multiobjective optimization, in *Proceeding of*, Ieee, pp. 82-87.

[35] J. Knowles, D. Corne, The pareto archived evolution strategy: A new baseline algorithm for pareto multiobjective optimisation, in *Proceeding of*, IEEE, pp. 98-105.

[36] E. Zitzler, L. Thiele, Multiobjective evolutionary algorithms: a comparative case study and the strength Pareto approach, *IEEE transactions on Evolutionary Computation*, Vol. 3, No. 4, pp. 257-271, 1999.

[37] K. Deb, J. Sundar, Reference point based multi-objective optimization using evolutionary algorithms, in *Proceeding of*, ACM, pp. 635-642.

[38] Moradi A, Shirazi KH, Keshavarz M, Falehi AD, Moradi M. Smart piezoelectric patch in non-linear beam: design, vibration control and optimal location. Transactions of the Institute of Measurement and Control. 2014 Feb;36(1):131-44.